

Ndr Effects in a Locally-Active Memristor Induce Small-Signal Amplification in a Simple Cell

Original

Ndr Effects in a Locally-Active Memristor Induce Small-Signal Amplification in a Simple Cell / Ascoli, A.; Gemo, E.; Corinto, F.; Bonnin, M.; Gilli, M.; Civalleri, P. P.; Demirkol, A. S.; Messaris, I.; Ntinis, V.; Prousalis, D.; Tetzlaff, R.; Slesazeck, S.; Mikolajick, T.; Chua, L.. - ELETTRONICO. - (2025), pp. 1-9. (Intervento presentato al convegno 2025 14th International Conference on Modern Circuits and Systems Technologies (MOCASST) tenutosi a Dresda (Ger) nel 11-13 June 2025) [10.1109/mocast65744.2025.11083728].

Availability:

This version is available at: 11583/3003071 since: 2025-09-15T19:34:54Z

Publisher:

IEEE

Published

DOI:10.1109/mocast65744.2025.11083728

Terms of use:

This article is made available under terms and conditions as specified in the corresponding bibliographic description in the repository

Publisher copyright

IEEE postprint/Author's Accepted Manuscript

©2025 IEEE. Personal use of this material is permitted. Permission from IEEE must be obtained for all other uses, in any current or future media, including reprinting/republishing this material for advertising or promotional purposes, creating new collecting works, for resale or lists, or reuse of any copyrighted component of this work in other works.

(Article begins on next page)

NDR Effects in a Locally-Active Memristor Induce Small-Signal Amplification in a Simple Cell

A. Ascoli, E. Gemo,
F. Corinto, M. Bonnin,
M. Gilli, P.P. Civalleri
*Department of Electronics
and Telecommunications,
Politecnico di Torino,
Torino, Italia
alon.ascoli@polito.it*

A.S. Demirkol, I. Messaris,
V. Ntinis, D. Prousalis,
R. Tetzlaff
*Institut für Grundlagen der
Elektrotechnik und
Elektronik, TU Dresden,
Dresden, Germany*

S. Slesazek^a,
T. Mikolajick^{a,b}
^a NaMLab gGmbH,
^b *Institut für Halbleiter- und
Mikrosystemtechnik,
TU Dresden,
Dresden, Germany*

L. Chua
*Department of Electrical
Engineering and Computer
Sciences,
University of California,
Berkeley, Berkeley,
California, USA*

Abstract—The Pt/NbO_x/Nb₂O₅/Pt threshold switch, manufactured at NaMLab, may admit a negative differential resistance (NDR). For example, this occurs when a constant voltage, let fall across a two-element one-port, composed of its series connection with a suitable linear resistor, stabilizes its bias point on a branch of the respective DC current-voltage characteristic, along which the slope assumes negative values. Around a bias point of this kind, the device may act as a source of local energy, justifying the *locally-active* attribute it is conferred. In past research studies the capability of the nanodevice to generate infinitesimal energy around a NDR bias point was exploited to induce the emergence of dramatic local phenomena in otherwise-dumb circuits, including the Hopf Supercritical and Pitchfork Bifurcations, which, while destabilizing a quiescent steady state, respectively spawn sine-wave-alike oscillations, or two new stable quiescent points, concurrently. In this research study, the local energy, which the switch releases about the NDR bias point, when a small-signal sine wave signal, superimposed on top of the DC stimulus, is applied across the two-element one-port, is leveraged to induce the development of larger oscillations across the resistor than those generated by the input source. While the key findings of our numerical investigations are provided here, the underlying theoretical analysis, supported by experimental verification, shall be reported in a Journal paper.

Keywords—Local Activity, Edge of Chaos, Threshold Switch, Small-Signal Amplification

I. INTRODUCTION

In recent years a large number of scientists across the globe have begun to direct the focus of research endeavors toward theoretical and practical aspects concerning particular classes of threshold switches ([1],[2]), a particular class of memristors showcasing a S-shaped DC current versus voltage characteristic. While being unable to store data for a very long time, differently from non-volatile resistance switching memories [3], these devices are however blessed with a negative differential resistance (NDR) [4] when poised along any bias point, where the DC current versus voltage characteristic is endowed with a negative slope. In fact, while sitting on a bias point of this kind, these devices are said to be *locally active* [5], since, under some suitable small-signal periodic perturbation, they may act as sources of infinitesimal energy. Their local activity may then be leveraged to induce various complex phenomena across analogue electrical cells, which would otherwise feature a trivial and uninteresting behavior. The NDR effects of a threshold switch of this kind, fabricated at NaMLab [6] and featuring a layer stack of the form Pt/NbO_x/Nb₂O₅/Pt, has been exploited to design bistable circuits, which were then used to explore and understand the

origin for symmetry-breaking phenomena, accompanied by the asymptotic formation of Turing patterns, in homogeneous reaction-diffusion systems from cellular biology [7], as well as to develop a novel compact and energy-efficient building block for Cellular Neural Networks [8]. While operating around a NDR bias point, a single NaMLab device may allow to reproduce the complex sequence of local and global bifurcations, underlying the life cycle of an Action Potential across neuronal axon membranes, in an electrical cell of unprecedented simplicity [9]. Last but not least, arrays of capacitively-coupled relaxation oscillators, each of which accommodating a single threshold switch, poised on the NDR branch of the respective DC characteristic, were found to outperform state-of-the-art hardware and software platforms in solving a computationally-hard optimization problem called graph coloring [10]. In this paper, the capability of the threshold switch to release an infinitesimal quantity of energy when, while continuously stabilized on a NDR bias point through a suitable one-DC-source-one-linear-resistor series one-port, placed across its terminals, an infinitesimal sine-wave voltage is superimposed on top of the bias stimulus, is employed to boost the local input signal. In particular, an in-depth numerical investigation revealed that the small-signal voltage oscillations, developing across the linear resistor in response to the infinitesimal purely-AC periodic perturbation, are larger than the input ones as long as the value assigned to the frequency is below a critical threshold. Due to lack of space, the mathematical analysis, gaining a complete understanding of the mechanisms underlying the exploitation of local energy production for voltage amplification in the proposed series circuit will be reported in a longer paper, where other counterintuitive phenomena, emerging in the elementary three-element cell, will also be disclosed and explained.

II. DEFINITION OF LOCAL ACTIVITY AND EDGE OF CHAOS

Let a n^{th} -order memristive one-port \mathcal{M} be excited by some input signal $u_{\mathcal{M}}$, composed of the sum between two components, specifically a DC level $U_{\mathcal{M}}$ and an infinitesimal signal $\delta u_{\mathcal{M}}$, which adds up to the constant stimulus, applied to the two-terminal electrical element first, from some later time instant t_0 . The state vector and output voltage (current) variable of the memristor in response to the excitation signal $u_{\mathcal{M}}$, assumed to be in current (voltage) form, will also consist of the sum between a constant component and a small-signal contribution, being respectively denoted as $\mathbf{x} \triangleq (x_1, \dots, x_n) = \mathbf{X} + \delta \mathbf{x}$ and $y_{\mathcal{M}} = Y_{\mathcal{M}} + \delta y_{\mathcal{M}}$. The one-port is

said to be *locally active* [5] about one operating point $\mathbf{Q}_{\mathcal{M}} \triangleq (Q_{1,\mathcal{M}} \equiv X_1, \dots, Q_{n,\mathcal{M}} \equiv X_n)$, at which it is preliminarily polarized through a certain DC stimulus $U_{\mathcal{M}} = \bar{U}_{\mathcal{M}}$, if and only if there exists a particular infinitesimal signal $\delta u_{\mathcal{M}}(t) = \delta u_{\mathcal{M}}^*(t)$, denoting a continuous function of time for all $t \geq t_0$, which triggers a state (output) solution to the memristor local model [6], featuring the initial condition $\delta \mathbf{x}(t_0) = \mathbf{0}$, in the form $\delta x(t) = \delta x^*(t)$ ($\delta y_{\mathcal{M}}(t) = \delta y_{\mathcal{M}}^*(t)$), such that, correspondingly, the infinitesimal energy $\delta \mathcal{E}_{\mathcal{M}}(t_0, t; \mathbf{Q}_{\mathcal{M}})$, absorbed by the memristive one-port over a time frame (t_0, t) , i.e.

$$\delta \mathcal{E}_{\mathcal{M}}(t_0, t; \mathbf{Q}_{\mathcal{M}}) = \int_{t_0}^t \delta u_{\mathcal{M}}^*(t') \cdot \delta y_{\mathcal{M}}^*(t') dt', \quad (1)$$

may assume a negative polarity at some time instant $t = \bar{t} > t_0$. Despite its rigor, this definition is not useful for testing purposes. Fortunately, however, the Local Activity Theorem serves this purpose. Transforming the memristor local model in the Laplace domain [6], some algebraic manipulation allows to derive a closed-form expression for its local transfer function $F_{\mathcal{M}}(s; \mathbf{Q}_{\mathcal{M}}) \triangleq (\mathcal{L}\{\delta y_{\mathcal{M}}(t)\} / \mathcal{L}\{\delta u_{\mathcal{M}}(t)\})|_{\mathbf{Q}_{\mathcal{M}}}$ about the respective operating point $\mathbf{Q}_{\mathcal{M}}$ ($\mathcal{L}\{\cdot\}$ denotes the Laplace transform operator). If $u_{\mathcal{M}}$ denotes the device voltage $v_{\mathcal{M}}$ (current $i_{\mathcal{M}}$), implying $y_{\mathcal{M}}$ to stand complementarily for the device current $i_{\mathcal{M}}$ (voltage $v_{\mathcal{M}}$), $F_{\mathcal{M}}(s; \mathbf{Q}_{\mathcal{M}})$ corresponds to the memristor local admittance $Y_{\mathcal{M}}(s; \mathbf{Q}_{\mathcal{M}})$ (impedance $Z_{\mathcal{M}}(s; \mathbf{Q}_{\mathcal{M}})$) about $\mathbf{Q}_{\mathcal{M}}$. The *Local Activity Theorem* [5] establishes that a n^{th} -order one-port is locally-active about an operating point $\mathbf{Q}_{\mathcal{M}}$ if and only if at least one of the four conditions to follow apply:

- 1) One pole of $F_{\mathcal{M}}(s; \mathbf{Q}_{\mathcal{M}})$, say the i^{th} one, denoted as $s = p_{i,F_{\mathcal{M}}}(\mathbf{Q}_{\mathcal{M}})$, where i may assume any integer value in the range $\{1, 2, \dots, n\}$, lies on the open Right Half Plane (RHP).
- 2) One pole of $F_{\mathcal{M}}(s; \mathbf{Q}_{\mathcal{M}})$, say the i^{th} one, denoted as $s = p_{i,F_{\mathcal{M}}}(\mathbf{Q}_{\mathcal{M}})$, where i may assume any integer value in the range $\{1, 2, \dots, n\}$, lies along the imaginary axis, i.e. $\Re\{p_{i,F_{\mathcal{M}}}(\mathbf{Q}_{\mathcal{M}})\} = 0$, while, concurrently, the respective residue, computed via $k_{p_{i,F_{\mathcal{M}}}(\mathbf{Q}_{\mathcal{M}})} \triangleq \lim_{s \rightarrow p_{i,F_{\mathcal{M}}}(\mathbf{Q}_{\mathcal{M}})} (s - p_{i,F_{\mathcal{M}}}(\mathbf{Q}_{\mathcal{M}})) \cdot F_{\mathcal{M}}(s; \mathbf{Q}_{\mathcal{M}})$, is either a negative real-valued number or a complex number.
- 3) $F_{\mathcal{M}}(s; \mathbf{Q}_{\mathcal{M}})$ admits l poles, say $s = p_{k,F_{\mathcal{M}}}(\mathbf{Q}_{\mathcal{M}})$, $s = p_{k+1,F_{\mathcal{M}}}(\mathbf{Q}_{\mathcal{M}})$, \dots , $p_{k+l-1,F_{\mathcal{M}}}(\mathbf{Q}_{\mathcal{M}})$, which lie along the $j\omega$ axis, where l denotes an integer from the set $\{2, \dots, n\}$, and defines the range, where k may fall into, i.e. $\{1, \dots, n - l + 1\}$.
- 4) The real part of $F_{\mathcal{M}}(s; \mathbf{Q}_{\mathcal{M}})$, evaluated for $s = j\omega$, assumes a negative value at some finite angular frequency $\omega = \omega_{0,F_{\mathcal{M}}}(\mathbf{Q}_{\mathcal{M}})$.

The *Edge of Chaos Corollary* [5] asserts that a n^{th} -order memristive one-port is *on the Edge of Chaos* about one operating point $\mathbf{Q}_{\mathcal{M}}$ if and only if two conditions simultaneously apply:

- 1) All the n poles of $F_{\mathcal{M}}(s; \mathbf{Q}_{\mathcal{M}})$ lie on the open Left Half Plane (LHP), i.e. $\Re\{p_{i,F_{\mathcal{M}}}(\mathbf{Q}_{\mathcal{M}})\} < 0$ for any integer value, assigned to the index i , from the set $\{1, 2, \dots, n\}$.
- 2) $\Re\{F_{\mathcal{M}}(j\omega; \mathbf{Q}_{\mathcal{M}})\}$ becomes negative at some finite angular frequency $\omega = \omega_{0,F_{\mathcal{M}}}(\mathbf{Q}_{\mathcal{M}})$.

Therefore, in order to be on the Edge of Chaos about a given operating point $\mathbf{Q}_{\mathcal{M}}$, the n^{th} -order one-port must necessarily be both locally active and asymptotically stable about it.

III. THE THRESHOLD SWITCH

Plots (a) and (b) in Fig. 1 respectively show a sketch and a Transmission Electron Microscope (TEM) image of the cross section of a volatile memristor [11], referred to as threshold switch [12] in the device physics community, manufactured at NaMLab [13], and featuring a layer stack of the form Pt/NbO_x/Nb₂O₅/Pt.

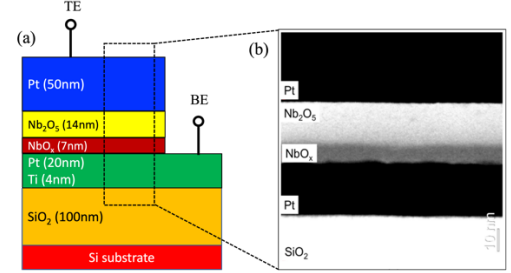


Fig. 1 (a) Sketch of the cross section of the threshold switch physical realization from NaMLab. The composition and thickness of each layer in the device stack are clearly indicated. BE (TE) is an acronym for bottom (top) electrode. (b) TEM image of one device sample, confirming the sequence of layers characterizing its physical structure.

The differential algebraic equation (DAE) [6] of the volatile memristor, is composed of a state equation reading as

$$\dot{x} = \dot{x}(x, v_{\mathcal{M}}) = a_0 + a_1 \cdot x + (b_2 + c_{21} \cdot x + c_{22} \cdot x^2 + c_{23} \cdot x^3 + c_{24} \cdot x^4 + c_{25} \cdot x^5) \cdot v_{\mathcal{M}}^2, \quad (2)$$

and of an Ohm-based law expressed by

$$i_{\mathcal{M}} = i_{\mathcal{M}}(x, v_{\mathcal{M}}) = G_{\mathcal{M}}(x) \cdot v_{\mathcal{M}}, \quad (3)$$

where x represents the state variable of the device, $i_{\mathcal{M}}$ ($v_{\mathcal{M}}$) the current (voltage) flowing (falling) through (across) its layer stack, and $G_{\mathcal{M}}(x)$ its memductance, depending upon the solution to equation (2) via

$$G_{\mathcal{M}}(x) = d_0 + d_1 \cdot x + d_2 \cdot x^2 + d_3 \cdot x^3 + d_4 \cdot x^4. \quad (4)$$

The values of the model parameters $a_0, a_1, b_2, c_{21}, c_{22}, c_{23}, c_{24}, c_{25}$ (d_0, d_1, d_2, d_3 , and d_4) in equation (2) ((4)) are reported in Table I.

Table I. Device model parameter setting. The physical units are omitted for simplicity.

a_0	a_1	b_2	c_{21}	c_{22}	c_{23}	c_{24}
$5.19 \cdot 10^9$	$-2.05 \cdot 10^7$	$7.21 \cdot 10^9$	$-7 \cdot 10^7$	$2.27 \cdot 10^5$	-240	0.125
c_{25}	d_0	d_1	d_2	d_3	d_4	
$-2.69 \cdot 10^{-5}$	$6.5 \cdot 10^{-3}$	$-6.66 \cdot 10^{-5}$	$2.14 \cdot 10^{-7}$	$-2.14 \cdot 10^{-10}$	$1.19 \cdot 10^{-13}$	

The model falls in the class of first-order voltage-driven generic memristors. However, from a circuit-theoretic perspective [14], it is a *current-controlled device*. In fact, as may be evinced by inspecting the device DC characteristic on the first quadrant of the voltage versus current plane¹, plotted in Fig. 2, each constant value $I_{\mathcal{M}}$, assigned to $i_{\mathcal{M}}$, maps to one and only one constant value $V_{\mathcal{M}}$ for $v_{\mathcal{M}}$. A red color is employed to indicate each bias point $P_{\mathcal{M}} = (I_{\mathcal{M}}, V_{\mathcal{M}})$, at which the DC characteristic features a negative slope, whose value corresponds in fact with the *negative differential resistance* (NDR) of the device therein. The device DC locus

¹ The DC characteristic of the threshold switch from NaMLab is odd symmetric [7]. Similar conclusions, as those to be discussed in this paper,

could be drawn *mutatis mutandis* on the basis of its properties in the third quadrant of the $V_{\mathcal{M}}$ versus $I_{\mathcal{M}}$ plane.

contains in fact three branches on the first quadrant of the V_M versus I_M plane. The red-colored solid NDR branch is sandwiched between two branches, along which the slope of the V_M versus I_M locus assumes positive values. When poised on a bias point P_M along the blue-colored (green-colored) solid branch, I_M is relatively small (large), and, as a result, especially in the device physics community the memristor is said to sit in a comparatively *high* (*low*) *resistance state*, HRS (LRS) for short. Concurrently, in either case, the device admits in P_M a *positive differential resistance* (PDR), whose value is given by the slope of the V_M versus I_M characteristic therein. Along the entire DC locus of Fig. 2 a bias point P_M corresponds to one and only one operating point Q_M for the current-controlled device. In its turn, Q_M is identically equal to the unique zero X of the state evolution function $\dot{x}(x, v_M)$ from equation (2), with $v_M = R_M(x) \cdot I_M$ and $R_M(x) = G_M^{-1}(x)$, when the current i_M , let flow through the device, is taken equal to a specific DC value I_M .

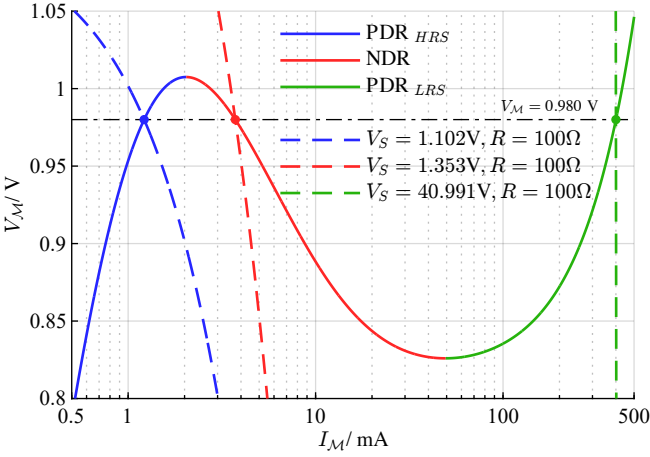


Fig. 2 DC characteristic of the NaMLab threshold switch. The NDR DC current, state, and voltage ranges respectively are $(I_{M,NDR,L}, I_{M,NDR,U}) = (2.037\text{mA}, 49.296\text{mA})$, $(Q_{M,NDR,L}, Q_{M,NDR,U}) = (350.894\text{K}, 1005.677\text{K})$, and $(V_{M,NDR,L}, V_{M,NDR,U}) = (0.826\text{V}, 1.007\text{V})$. NDR is an acronym for Negative Differential Resistance. The acronym PDR_{HRS} (PDR_{LRS}) stands for High (Low) Resistance State Positive Differential Resistance. The values along the horizontal axis are logarithmically scaled. The DC load line $V_m = V_S - V_R$ for the cell of Fig. 4, where $V_R = R \cdot I_M$, R is taken equal to 100Ω , and V_S is chosen as the first, second, and third value in the set $\{1.102\text{V}, 1.353\text{V}, 40.991\text{V}\}$ (refer in turn to the dashed blue, dashed red, and dashed green trace) crosses the DC V_M versus I_M locus in a single point P_M , featuring an ordinate of 0.980V and an abscissa of 1.217mA , 3.731mA , and 400.088mA , respectively. Importantly, for $V_S = 1.353\text{V}$, the abscissa of P_M falls inside the NDR DC current range.

Table II reports the expressions for the device small-signal or local model parameters in terms of its operating point Q_M .

Table II. Formulas for the memristor local model parameters about Q_M .

$a(Q_M) \triangleq (\partial \dot{x} / \partial x) _{Q_M}$
$a_1 + V_M^2 \cdot (c_{21} + 2 \cdot c_{22} \cdot X + 3 \cdot c_{23} \cdot X^2 + 4 \cdot c_{24} \cdot X^3 + 5 \cdot c_{25} \cdot X^4)$
$b(Q_M) \triangleq (\partial \dot{x} / \partial v_M) _{Q_M}$
$2 \cdot (b_2 + c_{21} \cdot X + c_{22} \cdot X^2 + c_{23} \cdot X^3 + c_{24} \cdot X^4 + c_{25} \cdot X^5) \cdot V_M$
$c(Q_M) \triangleq (\partial i_M / \partial x) _{Q_M}$
$(d_1 + 2 \cdot d_2 \cdot X + 3 \cdot d_3 \cdot X^2 + 4 \cdot d_4 \cdot X^3) \cdot V_M$
$d(Q_M) \triangleq (\partial i_M / \partial v_M) _{Q_M}$
$G_M(X)$

One of the possible circuit-theoretic representations [15] for the switch local model about Q_M is illustrated in Fig. 3,

where A and B correspond to the top and bottom electrodes in Fig. 1, respectively. The device small-signal impedance $Z_M(s; Q_M)$ of the threshold switch \mathcal{M} about Q_M may be cast in the form

$$Z_M(s; Q_M) = K_{Z_M}(Q_M) \cdot \frac{s - z_{Z_M}(Q_M)}{s - p_{Z_M}(Q_M)}, \quad (5)$$

where the formulas for the scaling factor K_{Z_M} , the zero z_{Z_M} , and the pole p_{Z_M} are given in Table III.

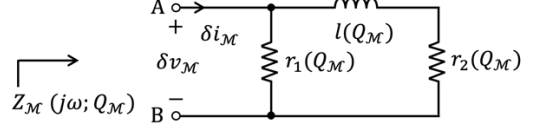


Fig. 3 Small-signal equivalent circuit model of the NaMLab threshold switch \mathcal{M} about an operating point Q_M .

Table III. Formulas for the three Q_M -dependent parameters in equation (5), describing the impedance of the circuit of Fig. 3 at the port A-B.

$K_{Z_M}(Q_M) = r_1(Q_M)$
$z_{Z_M}(Q_M) = -r_2(Q_M)/l(Q_M)$
$p_{Z_M}(Q_M) = -(r_1(Q_M) + r_2(Q_M))/l(Q_M)$
$r_1(Q_M) = 1/d(Q_M)$
$r_2(Q_M) = -a(Q_M)/(b(Q_M) \cdot c(Q_M))$
$l(Q_M) = 1/(b(Q_M) \cdot c(Q_M))$

While $r_1(Q_M)$ and $l(Q_M)$ are strictly positive, $r_2(Q_M)$ goes negative across the NDR branch of the device DC characteristic of Fig. 2, keeping positive elsewhere (the device negative differential resistance is in fact computable via $r(Q_M) \equiv Z_M(0; Q_M) \triangleq r_1(Q_M) \parallel r_2(Q_M)$). Taking also into account that the sum between the two resistances in the circuit of Fig. 3 is positive irrespective of Q_M , invoking the Local Activity Theorem [5], it is possible to conclude that the threshold switch \mathcal{M} is on the Edge of Chaos [6] anywhere along the NDR branch of the respective DC characteristic, whereas it is locally passive at any bias point P_M from either of the two PDR branches of the V_M versus I_M locus.

IV. LOCAL VOLTAGE AMPLIFICATION

A. The Small Signal Amplification Cell and Its DC Energy Supply

In this work the capability of the NaMLab memristor to deliver an infinitesimal amount of energy when poised on a bias point P_M , lying along the red-colored solid NDR branch of the DC V_M versus I_M characteristic of Fig. 2, is leveraged to amplify a periodic voltage signal $\delta v_S = \hat{v}_S \cdot \sin(2 \cdot \pi \cdot f \cdot t)$, oscillating at some frequency f with a tiny amplitude \hat{v}_S around a suitable DC level V_S , in the three-element series circuit shown in Fig. 4. This circuit accommodates a linear resistor of resistance R and the source, generating the overall stimulus $v_S = \delta v_S + V_S$, besides the threshold switch. Let us provide a proof of evidence for the necessity for the memristor to sit on a NDR bias point P_M in order for this first-order analogue electrical cell to act as a small signal amplifier under local sine wave stimulation. With reference to Fig. 2, when the value for V_M falls within the NDR DC voltage range $(V_{M,NDR,L}, V_{M,NDR,U}) = (0.826\text{V}, 1.007\text{V})$, the bias current I_M can in principle assume each of three admissible levels. For example, with $V_M = 0.980\text{V}$, the bias point P_M of the threshold switch \mathcal{M} could lie on the high resistance state PDR (PDR_{HRS}) branch, on the NDR branch, or on the low resistance state PDR (PDR_{LRS}) branch of the DC locus from Fig. 2. The first, second, and third option

would occur when the current I_M , flowing between the device terminals, were in turn equal to 1.217mA, 3.731mA, and² 400.088mA. Letting the current i_M flowing through the device to the first, second, and third DC value I_M in this triplet would be sufficient to poise the device on the bias point P_M marked through a blue, red and green circle marker in Fig. 2, respectively.

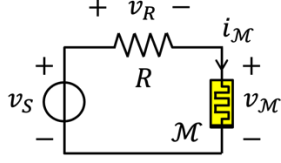


Fig. 4 First-order cell under study. It consists of the series combination between one voltage source v_S , composed of the sum between a DC component V_S and a sine wave signal δv_S of infinitesimal amplitude \hat{v}_S and frequency f , one linear and passive resistor R , and one globally-passive yet locally-active memristor \mathcal{M} . After transients vanish, the memristor state, voltage and current may be cast in the form $x = X + \delta x$, $v_M = V_M + \delta v_M$, and $i_M = I_M + \delta i_M$, respectively. Similarly, the steady-state voltage across the resistor may be expressed via $v_R = V_R + \delta v_R$.

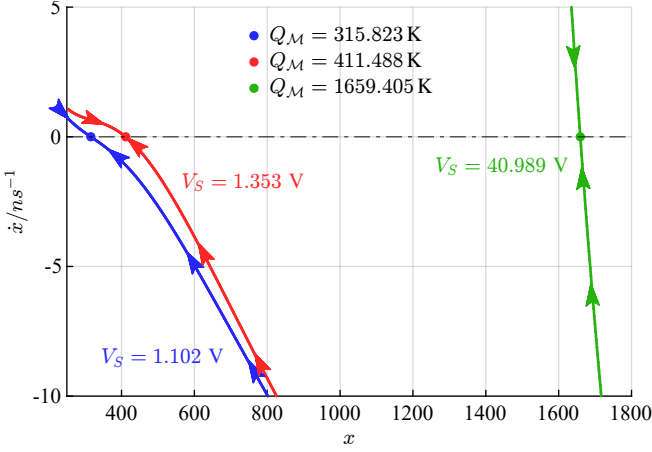


Fig. 5 Blue, red, and green trace: Locus of $\dot{x} = g(x, v_M(x))$ versus x with $v_M(x) = V_S / (1 + R \cdot G_M(x))$ for $R = 100\Omega$, when the first, second, and third value from the set $\{1.102V, 1.353V, 40.991V\}$ is assigned to the DC voltage stimulus V_S in the cell of Fig. 4. The arrows, superimposed along each locus, which, as a result, is referred to as a State Dynamic Route (SDR), indicate the direction of motion of the state variable x from any initial condition $x_0 \triangleq x(0)$ over the course of the transients, which the cell experiences in the corresponding simulation scenario. Irrespective of the initial condition, when V_S is set to the first, second, and third value in the aforegiven triplet, the unique operating point $Q_M = X$, the state x is found to settle eventually onto, is found to be equal to 315.823K, 411.488K, and 1659.405K, respectively. Importantly, for $V_S = 1.353V$, the value of Q_M falls inside the NDR DC state range $(Q_{M,NDR,L}, Q_{M,NDR,U}) = (350.894K, 1005.677K)$.

Alternatively, the memristor \mathcal{M} may be stabilized on the first, second, and third bias point P_M from this triplet through the cell of Fig. 4, where, fixing R to a sufficiently high value, e.g. 100Ω [2], the value assigned to V_S , computable through the DC load line formula $V_S = V_m + R \cdot I_m$, is taken equal to 1.102V, 1.353V, and 40.991V, respectively. In the first, second, and third case, the constant level Q_M , the memristor volatile state x would be found to converge toward, after transients fade away, is in turn 315.823K, 411.488K, and

1659.405K, as predicted through the State Dynamic Route (SDR) analysis of Fig. 5.

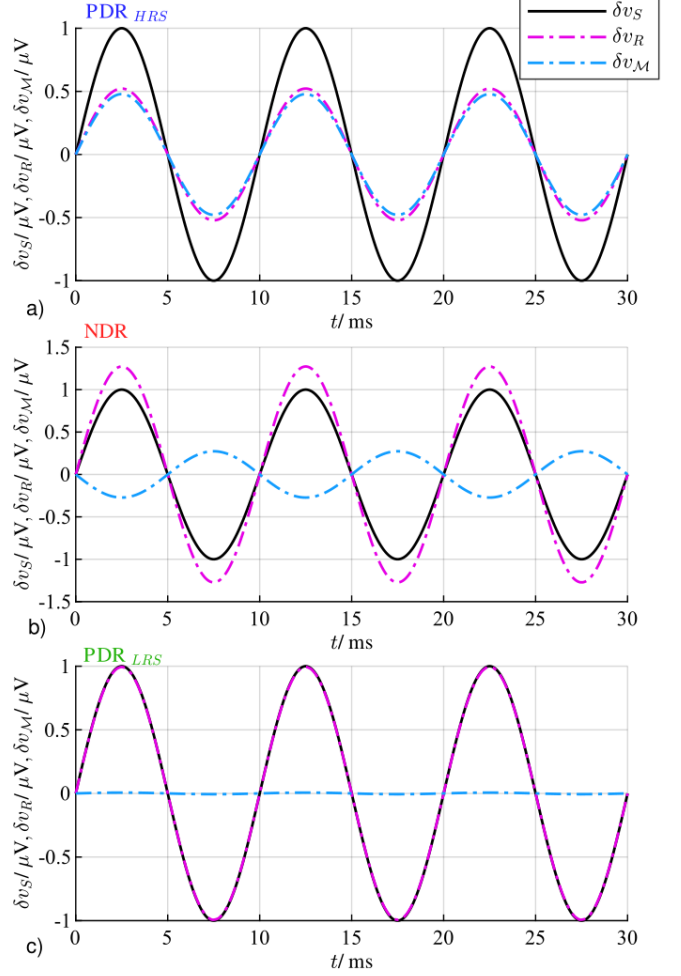


Fig. 6 (a)-(c) Steady-state temporal waveforms of the local voltages δv_M and δv_R , falling respectively across the memristor (dashed cyan trace) and the resistor (dashed magenta trace) in response to a small-signal sine-wave voltage excitation signal δv_S (solid black trace) of amplitude $\hat{v}_S = 1\mu V$ and frequency $f = 100Hz$, for three different scenarios, i.e. under the hypothesis that, concurrently, with R fixed to 100Ω , a DC input voltage V_S of 1.102V, 1.353V, or 40.991V stimulates the cell of Fig. 4. In the first, second, and third scenario, illustrated in turn in plot (a), (b), and (c), \mathcal{M} is poised on the bias point P_M marked through a blue, a red, and a green circle in Fig. 2, respectively. An appropriate shift has been applied to the steady-state time data series in such a way to relocate its first point at the origin. While these simulation results have been obtained via numerical integration of the DAE set (6)-(7), they agree with the numerical solutions of the respective small-signal model, being $\hat{v}_S \ll V_S$ for each of the three case studies illustrated in plots (a), (b), and (c).

B. Unfolding the Cell' Small Signal Amplification Capabilities

Fig. 6 (7), obtained by simulating the large-signal DAE model of the cell of Fig. 4, i.e.

$$\dot{x} = \dot{x}(x, v_M), \quad (6)$$

and

$$v_M = \frac{1}{1+R \cdot G(x)} \cdot v_S, \quad (7)$$

where the functional form of $\dot{x}(\cdot, \cdot)$ is reported in equation (2), shows the local voltages δv_M (dashed cyan trace) and δv_R (dashed magenta trace), developing at steady state across the

² While a high DC current of this kind would definitely jeopardize the lifetime of the threshold switch, the numerical exploration of the local behavior of the threshold switch around the PDR_{LRS} bias point under consideration under small-signal sine-wave excitation is however intended

to demonstrate the impossibility for the cell of Fig. 4 to boost the amplitude of the infinitesimal stimulus when the device is poised anywhere along the green branch of the V_M versus I_M characteristic of Fig. 2.

memristor and the resistor, respectively, under the application of a sine-wave voltage stimulus δv_S (solid black trace) of small-signal amplitude $\hat{v}_S = 1\mu\text{V}$ and frequency $f = 100\text{Hz}$ ($f = 10\text{MHz}$) in each of the three distinct scenarios, depicted in turn in plots (a), (b), and (c), where the threshold switch is poised at the bias point P_M lying on the PDR_{HRS} branch at $(1.217\text{mA}, 0.980\text{V})$, on the NDR branch at $(3.731\text{mA}, 0.980\text{V})$, and on the PDR_{LRS} bias point at $(400.088\text{mA}, 0.980\text{V})$, as illustrated earlier in Fig. 2.

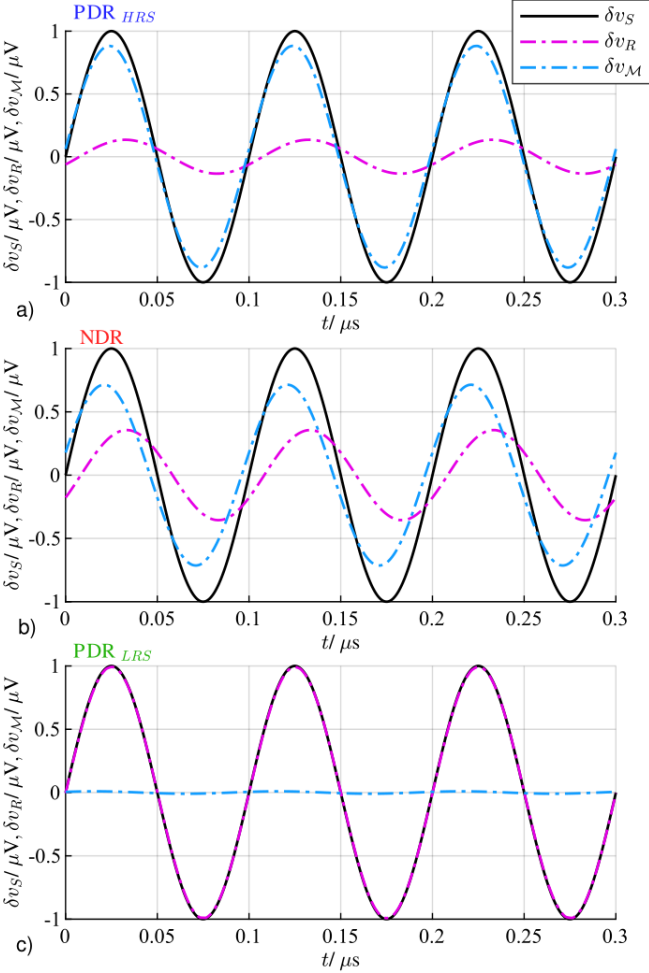


Fig. 7 (a), (b), (c) Time course of the small-signal voltages δv_M and δv_R , falling after transients fade away, across \mathcal{M} (dashed cyan trace) and R (dashed magenta trace), respectively, in response to a periodic voltage stimulus δv_S of sinusoidal form (solid black trace), infinitesimal amplitude $\hat{v}_S = 1\mu\text{V}$, and frequency $f = 10\text{MHz}$, for three distinct scenarios, i.e. under the assumption that, simultaneously, a DC input voltage V_S of 1.102V , 1.353V , or 40.991V excites the cell of Fig. 4, where R is kept equal to 100Ω . In the first, second, and third scenario, shown in turn in plot (a), (b), and (c), the memristor operates around the bias point P_M indicated through a blue, a red, and a green circle in Fig. 2, respectively. A suitable shift has been applied to the steady-state time data series for its first point to appear at the origin. Once again, the simulation results, recorded via numerical integration of the DAE set (6)-(7) agree with the solutions to the respective small-signal model, being $\hat{v}_S \ll V_S$ in each of the case studies from plots (a), (b), and (c).

Inspecting the plots in Figs. 6 and 7, it is easy to realize that the amplitude \hat{v}_R of the infinitesimal periodic voltage waveform δv_R , dropping across the resistor at steady state, is larger than the amplitude \hat{v}_S of the small-signal sine-wave voltage stimulus δv_S only when the memristor is poised on the NDR bias point $P_M = (3.731\text{mA}, 0.980\text{V})$ and the input frequency is chosen equal to 100Hz . On the other hand, the amplitude \hat{v}_M of the periodic voltage δv_M , falling across the memristor after transients decay to zero, is found to be smaller

than unity in all cases. Figs. 8 and 9, extracted from the numerical simulations of the DAE set (6)-(7), which produced the results visualized in Figs. 6 and 7, respectively, show the time course of the instantaneous local powers δp_S (black trace), δp_M (teal trace), and δp_R (magenta trace) absorbed at steady state by the local voltage source, by the memristor, and by the resistor, in the scenario where the frequency f of the small-signal sine-wave stimulus is in turn set to 100Hz and 10MHz . In each of Figs. 8 and 9, plots (a), (b), and (c) illustrate the case where the memristor is poised on a bias point P_M lying at $(1.217\text{mA}, 0.980\text{V})$, at $(3.731\text{mA}, 0.980\text{V})$, and at $(400.088\text{mA}, 0.980\text{V})$ of the V_M versus I_M characteristic, respectively. Importantly, only when the threshold switch from NaMLab is stabilized on the NDR bias point, and for the lower input frequency case, does the memristor absorb a negative amount of local energy per cycle, as may be inferred by inspecting plot (b) of Fig. 8. This indicates that the capability of the memristor to generate an infinitesimal amount of energy about $Q_M = 411.488\text{K}$ across each cycle of a suitable small-signal sine-wave stimulus allows to obtain local voltage gain across the resistor, relative to the input port, in the three-element series circuit of Fig. 4.

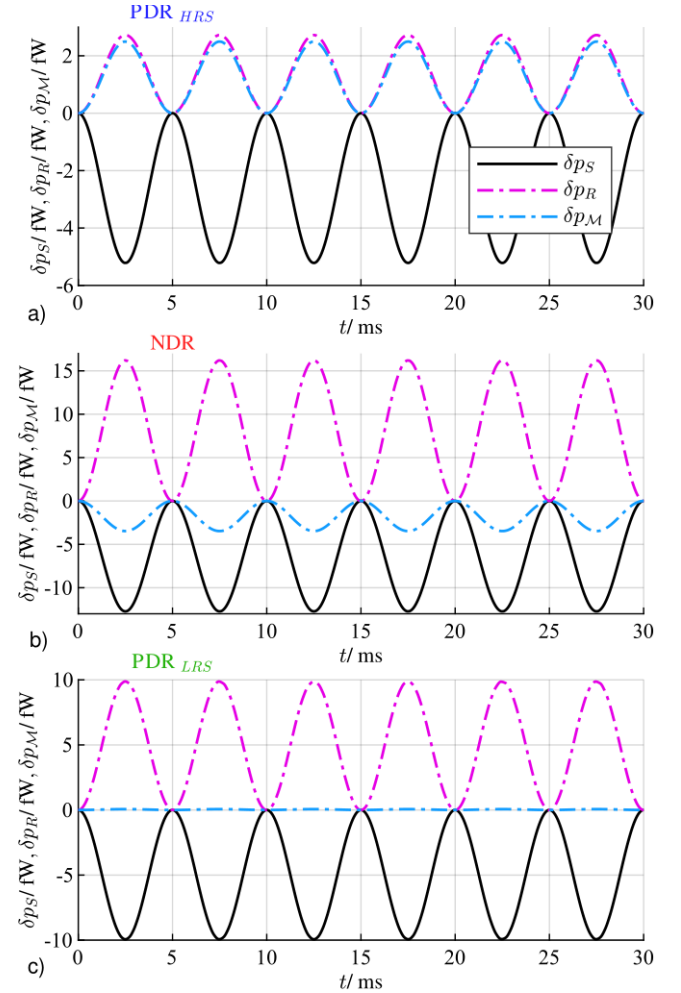


Fig. 8 (a), (b), (c) Time waveforms of the instantaneous local powers absorbed respectively by the voltage source (black trace), the memristor (teal trace), and the resistor (magenta trace) in the cell of Fig. 4, when, with R fixed to 100Ω , V_S is respectively set to 1.102V , 1.353V , and 40.991V , while the amplitude and frequency of the sine-wave input signal, oscillating around such bias level, are in turn chosen as $1\mu\text{V}$ and 100Hz .

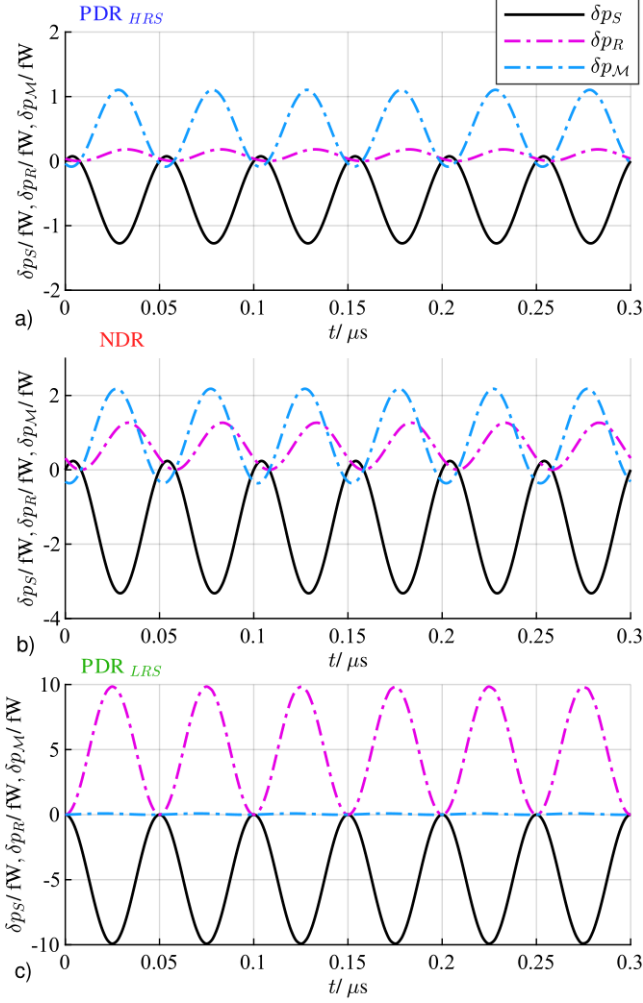


Fig. 9 (a), (b), (c) Temporal trends of δp_s (black trace), δp_M (teal trace), and δp_R (magenta trace) recorded at steady state in the cell of Fig. 4, when, with R kept equal to 100Ω , V_S is in turn chosen as $1.102V$, $1.353V$, and $40.991V$, while the values $1\mu V$ and $10MHz$ are assigned to \hat{v}_s and f , respectively.

Let us define the dimensionless *resistor-referred local transfer function* $H_R(s; Q_M)$ as the ratio between the Laplace transform of δv_R and the Laplace transform of δv_S when the memristor sits at the operating point Q_M , i.e. as

$$H_R(s; Q_M) \triangleq \frac{\mathcal{L}\{\delta v_R(t)\}}{\mathcal{L}\{\delta v_S(t)\}} \Big|_{Q_M} = \frac{R}{R + Z_M(s; Q_M)}, \quad (8)$$

whose expression in terms of the memristor local impedance $Z_M(s; Q_M)$ at Q_M , reported in equation (5), was derived by applying the circuit-theoretic voltage division rule [14] to the cell of Fig. 4. Importantly, $H_R(s; Q_M)$ also expresses the ratio between \hat{v}_R and \hat{v}_S when, as is the case here, the local AC behavior of the cell large-signal model, reported in equations (6)-(7), is approximated in a fairly accurate way by the DAE set variant obtained through its linearization about Q_M [16]. The magenta and teal traces in Fig. 10 respectively illustrate the loci of the modulus $|H_R(s; Q_M)|$ and of the phase $\angle H_R(s; Q_M)$ of the resistor-referred local transfer function $H_R(s; Q_M)$, evaluated for $s = j\omega$, versus the frequency $f = \omega/(2\pi)$, for the scenarios, where the memristor operating point Q_M is in turn stabilized at $315.823K$ (plot (a)), at $411.488K$ (plot (b)), and at $1659.405K$ (plot (c)) in the cell of Fig. 4, where, with $R = 100\Omega$, V_S is correspondingly set to $1.102V$, $1.353V$, and $40.991V$. Clearly, $|H_R(j\omega; Q_M)|$ is found to be larger than 1 only for $Q_M = 411.488K$, and provided the frequency f is smaller than a critical threshold

$f_{|H_R|=1}(Q_M)$ equal to $1.508MHz$ (see the hollow magenta square marker in plot (b)). The blue trace shows the locus of the phase $\angle Z_M(j\omega; Q_M)$ of the memristor local impedance $Z_M(j\omega; Q_M)$ at Q_M . It is important to point out that $\angle Z_M(j\omega; Q_M)$ keeps above $\pi/2$, i.e., equivalently, $\Re\{Z_M(j\omega; Q_M)\}$ features a negative sign, for all frequencies below another critical threshold $f_{\angle Z_M=\pi/2}(Q_M)$, which is here equal to $2.428MHz$ (see the hollow blue square marker in plot (b)).

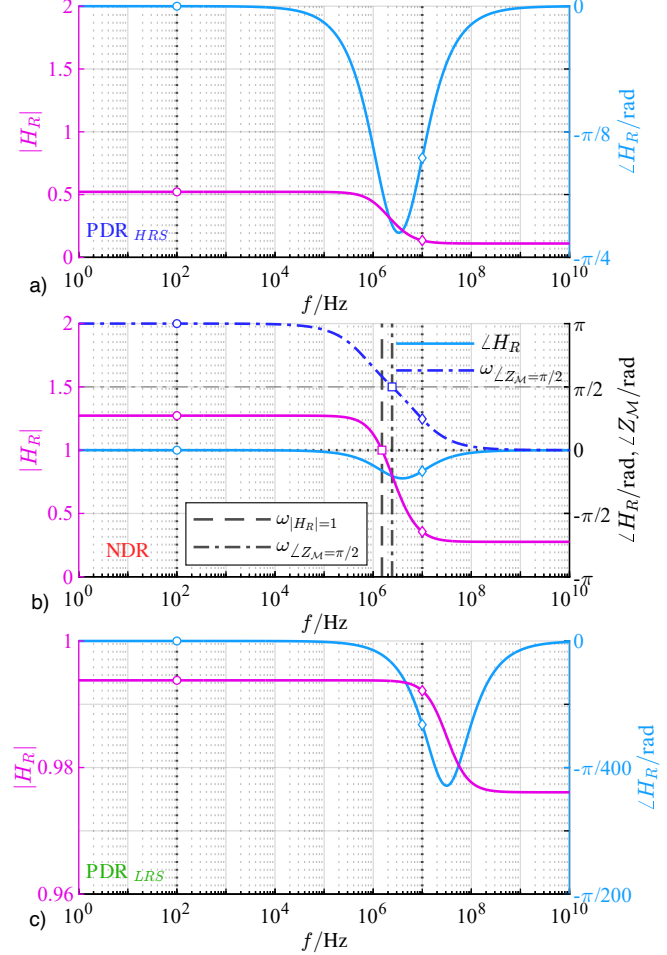


Fig. 10 (a), (b), and (c) Locus of the modulus $|H_R(j\omega; Q_M)|$ (magenta trace) and of the phase $\angle H_R(j\omega; Q_M)$ (teal trace) of the resistor-referred local transfer function $H_R(j\omega; Q_M)$ as a function of the frequency $f = \omega/(2\pi)$ for the scenario where the memristor is respectively polarized on the first, second, and third operating point Q_M from the set $\{315.823K, 411.488K, 1659.405K\}$ in the cell of Fig. 4, where R is fixed to 100Ω , whereas the DC voltage stimulus V_S is in turn taken equal to $1.102V$, $1.353V$, and $40.991V$. Importantly, $|H_R(j\omega; Q_M)|$ may exceed unity only when $Q_M = 411.488K$. Moreover, as may be evinced by visual inspection of plot (b), this is the case only for each frequency f below a critical threshold $f_{|H_R|=1}(Q_M)$, here equal to $1.508MHz$, which, rather interestingly, is lower than the frequency $f_{\angle Z_M=\pi/2}(Q_M)$, found to be equal to $2.428MHz$, at which the phase $\angle Z_M(j\omega; Q_M)$ of the memristor local impedance $Z_M(j\omega; Q_M)$ about Q_M (refer to the blue trace) descends down to $\pi/2$. In each of the three plots magenta and teal hollow circles (diamonds) respectively indicate the values of the modulus and of the phase of the resistor-referred local transfer function about the associated memristor operating point for $f = 100Hz$ ($f = 10MHz$). With reference to plot (b) the magenta hollow square marker is located on the graph of $|H_R(j\omega; Q_M)|$ as it descends down to 1 at the frequency $f_{|H_R|=1}(Q_M) = 1.508MHz$. In the same plot the blue hollow circle, square, and diamond markers show the values for the phase of the memristor local impedance about $Q_M = 411.488K$ at $f = 100Hz$, as it descends down to $\pi/2$ at $f_{\angle Z_M=\pi/2}(Q_M) = 2.428MHz$, and at $f = 10MHz$, respectively.

Since $f_{|H_R|=1}(Q_M) < f_{\angle Z_M=\pi/2}(Q_M)$, the input frequency f of the small-signal sine-wave voltage stimulus must be chosen

across a subset of the range of frequencies, across which $\Re\{Z_M(j\omega; Q_M)\}$ goes negative, for the infinitesimal oscillations in the voltage, falling across the resistor at steady state in the cell of Fig. 4, as a result, to be larger than the input oscillations. The frequency of 100Hz (10MHz) – see the hollow magenta square (diamond) – clearly falls inside (outside) such subset, as expected from the numerical simulation result in plot (b) of Fig. 8 (9).

For the sake of complexity, let us define the *memristor-referred local transfer function* $H_M(s; Q_M)$ as the ratio between the Laplace transform of $\delta v_M(t)$ and the Laplace transform of $\delta v_S(t)$ when the memristor sits at the operating point Q_M , i.e. as

$$H_M(s; Q_M) \triangleq \frac{\mathcal{L}\{\delta v_M(t)\}}{\mathcal{L}\{\delta v_S(t)\}} \Big|_{Q_M} = \frac{Z_M(s; Q_M)}{R + Z_M(s; Q_M)}. \quad (9)$$

$H_M(s; Q_M)$ also corresponds to the ratio between \hat{v}_M and \hat{v}_S when, as is the case here, the local AC behavior of the cell of Fig. 4 is approximated rather accurately by its small-signal variant about Q_M , obtained from the large-signal circuit by replacing the memristor with its local impedance at the operating point and turning the DC stimulus off. The magenta and teal traces in Fig. 11 show in turn the graphs of the modulus $|H_M(s; Q_M)|$ and of the phase $\angle H_M(s; Q_M)$ of the memristor-referred local transfer function $H_M(s; Q_M)$, computed for $s = j\omega$, against the frequency f , for the scenarios, where the memristor operating point Q_M is respectively stabilized at 315.823K (plot (a)), at 411.488K (plot (b)), and at 1659.405K (plot (c)) in the cell of Fig. 4, where, with R fixed to 100 Ω , V_S is taken equal to 1.102V, 1.353V, and 40.991V, correspondingly. Clearly, $|H_M(s; Q_M)|$ keeps below unity even for $Q_M = 411.488K$, where for each frequency below $f_{\angle Z_M = \pi/2}(Q_M) = 2.428\text{MHz}$, $\Re\{Z_M(j\omega; Q_M)\}$ admits a negative polarity.

Keeping now the resistance of the resistor R at 100 Ω , and stepping the value, assigned to the DC input voltage V_S , across the range (0.5V, 50V), the upper part of which is of purely-theoretical interest (recall footnote 2), the modulus of the resistor-referred local transfer function $H_R(j\omega, Q_M)$, evaluated at a frequency f of 100Hz, is found to be larger than positive one if and only if the memristor bias point P_M falls along the solid red-colored NDR branch of the DC V_M versus I_M locus of Fig. 2, i.e. as long as the value for V_S is comprised between 1.211V and 5.750V, as demonstrated in Fig. 12(a). On the other hand, concurrently, no local voltage gain, relative to the input port, may ever be extracted across the memristor, irrespective of the bias input voltage, as showcased in Fig. 12(b). Importantly, as long as V_S falls inside the interval (1.211V, 5.750V), where, correspondingly, for $R = 100\Omega$, Q_M lies within the NDR DC state range $(Q_{M,NDR,L}, Q_{M,NDR,U}) = (350.894K, 1005.677K)$, the local sine-wave voltage stimulus δv_S , appearing at the input port and featuring a sufficiently-small amplitude \hat{v}_S , e.g. 1 μV as in Figs. 6 and 7, is bound to be boosted across the resistor, providing its frequency f is lower than the ordinate of the relevant point along the $\omega_{|H_R|=1}(Q_M)$ versus V_S locus (violet-colored solid trace), as visualized in Fig. 12(c). Interestingly, keeping the focus on this plot, the violet-shaded area, denoting the region of the ω versus V_S parameter plane, where the local sine-wave input voltage is amplified across the resistor port, lies completely inside the teal-shaded area, enclosed by the horizontal axis and by the $\omega_{\angle Z_M = \pi/2}(Q_M)$ versus V_S locus (teal-colored dashed trace), showing the region of the same

plane, where $\angle Z_M(j\omega; Q_M)$ is larger than $\pi/2$. An in-depth analytical work, shedding light into the intricacies of the local voltage amplification capability of the three-element cell of Fig. 4, and unveiling additional counterintuitive nonlinear dynamical phenomena, emerging across its circuitry, will be reported shortly in a Journal paper.

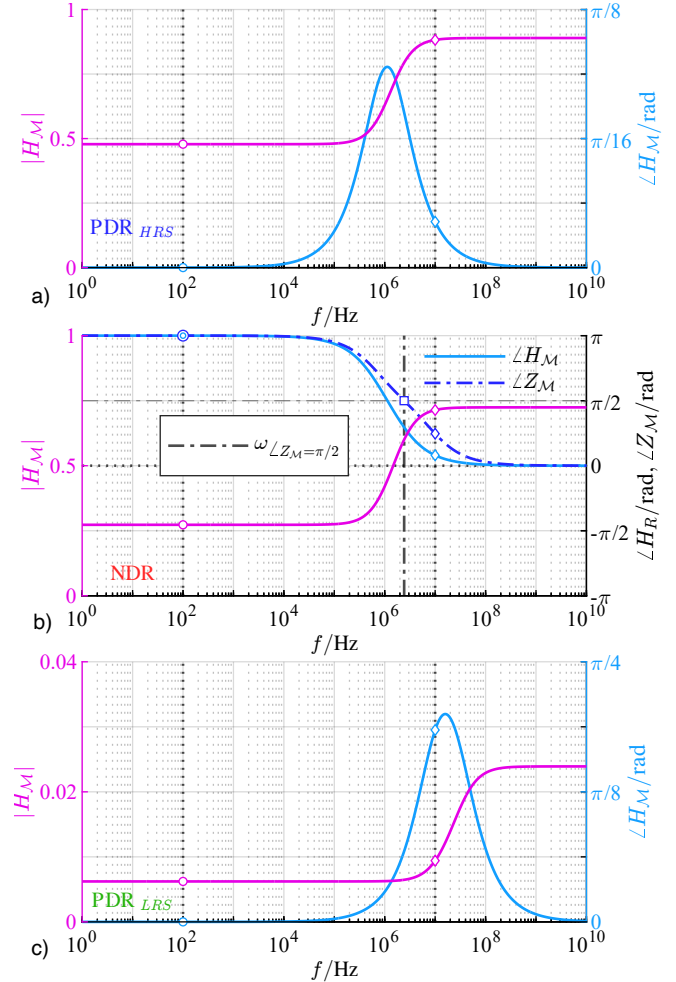


Fig. 11 (a), (b), (c) Graphical illustration for the dependence of the modulus $|H_M(j\omega; Q_M)|$ (magenta trace) and of the phase $\angle H_M(j\omega; Q_M)$ (teal trace) of the memristor-referred local transfer function $H_M(j\omega; Q_M)$ upon the frequency f for the scenario where the memristor is correspondingly poised on the first, second, and third operating point Q_M from the set $\{315.823K, 411.488K, 1659.405K\}$ in the cell of Fig. 4, where R is kept equal to 100 Ω , whereas the values of 1.102V, 1.353V, and 40.991V, are respectively assigned to the DC voltage stimulus V_S . Irrespective of the memristor polarization, $|H_M(j\omega; Q_M)|$ never exceeds unity. This does not even occur in plot (b), where the phase of the memristor local impedance, computable via $\angle Z_M(j\omega; Q_M) = \angle H_M(j\omega; Q_M) - \angle H_R(j\omega; Q_M)$, about $Q_M = 411.488K$ (blue trace), is found to be negative for frequencies below $f_{\angle Z_M = \pi/2}(Q_M) = 2.428\text{MHz}$. In each of the three plots magenta and teal hollow circles (diamonds) respectively show the values of the modulus and of the phase of the memristor-referred local transfer function about the relevant memristor operating point for $f = 100\text{Hz}$ ($f = 10\text{MHz}$). The blue hollow circle, square, and diamond markers in plot (b) indicate the values for the phase of the memristor local impedance about $Q_M = 411.488K$ at $f = 100\text{Hz}$, at $f_{\angle Z_M = \pi/2}(Q_M) = 2.428\text{MHz}$, when it descends down to $\pi/2$, and at $f = 10\text{MHz}$, correspondingly.

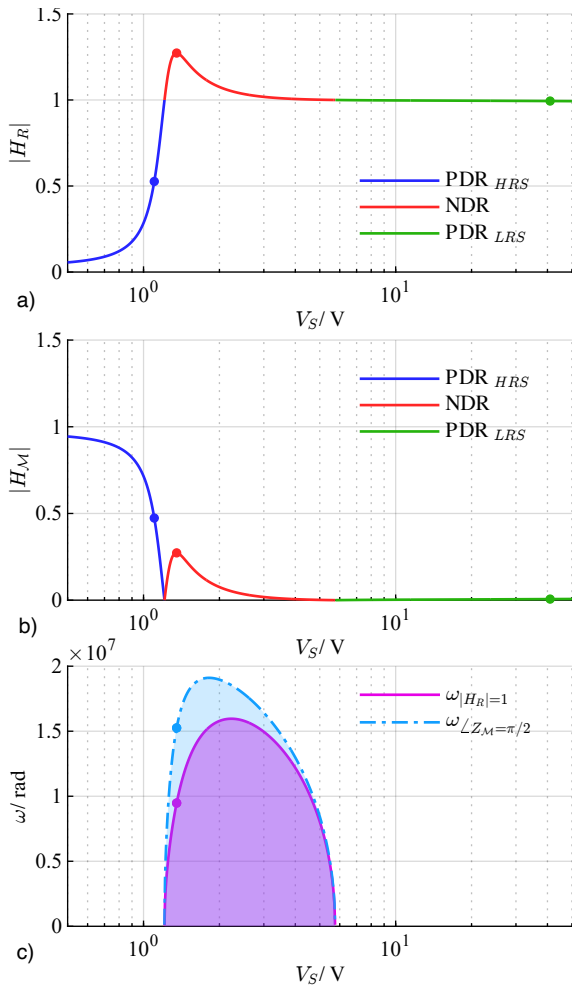


Fig. 12 (a), (b) Modulus of the resistor-referred and memristor-referred local transfer functions $H_R(j\omega; Q_M)$ and $H_M(j\omega; Q_M)$, evaluated at a frequency f of 100Hz about each operating point Q_M , the memristor in the cell of Fig. 4 is stabilized at, when, with R set to 100Ω , V_S is stepped from 0.5V to 50V. In the first (latter) plot the ordinates of the blue, red and green circles indicate the ratio between \hat{v}_R (\hat{v}_M) and \hat{v}_S in the steady-state simulation results from plots (a), (b), and (c) of Fig. 6 (7), respectively. (c) Teal-colored dashed trace: Locus of $\omega_{\angle Z_M=\pi/2}$ versus V_S for $R = 100\Omega$. Teal-shaded area: region of the ω versus V_S parameter plane, across which $\angle Z_M(j\omega; Q_M)$ is larger than $\pi/2$ for $R = 100\Omega$. Teal circle: $\omega_{\angle Z_M=\pi/2}$ for $V_S = 1.353V$. Violet-colored solid trace: Locus of $\omega_{|H_R|=1}$ versus V_S for $R = 100\Omega$. Violet-shaded area: region of the ω versus V_S parameter plane, across which the local sine-wave input voltage is amplified across the resistor port for $R = 100\Omega$. Violet circle: $\omega_{|H_R|=1}$ for $V_S = 1.353V$.

V. CONCLUSION

Major recent advances in material engineering enable the fabrication of non-volatile memristive devices with exceptional data storage capabilities [17]-[18]. Moreover, another class of memristors, referred to as threshold switches [1], and unable to retain information under power-off conditions, attract much interest in the scientific community. Being endowed with a non-monotonic S-shaped DC characteristic on the current versus voltage plane, similarly as the sodium and potassium ion channels [19] across neuronal axon membranes, these volatile memristors naturally enable the circuit implementation of bio-inspired computing paradigms [20]-[21]. When poised on some bias point, where the DC characteristic features a negative slope, a threshold switch is found to admit a Negative Differential Resistance (NDR), and acquires, as a result, the extraordinary capability

to act as a source of infinitesimal energy. The local energy production functionality of a volatile memristor physical realization from NaMLab [13] has been exploited to induce local bifurcations, resulting in counterintuitive emergent phenomena across physical cellular systems, in analogue electrical cells featuring topologies simpler than the biological counterparts [22]. In a more recent study, the NDR effects, emerging across the NaMLab threshold switch, have been leveraged to trigger the sequence of three fundamental bifurcations, dictating the salient phases in the life cycle of an electrical voltage spike across neuronal axon membranes, in an elementary cell including additionally only one capacitor and one current source [9]. In this paper, we reveal another more natural way [23]-[24] to take advantage of the local energy release ability of the NaMLab memristor [6] demonstrating, by means of numerical investigations, to be followed up shortly by a comprehensive theoretical explanation, how it enables to boost the strength of a small-signal sine-wave stimulus, superimposed on top of a suitable polarization level, in a three-element series circuit, in which the input (output) port is taken across a voltage source (a linear and passive resistor).

ACKNOWLEDGMENT

The research study, presented in this paper, has been financially supported by the Deutsche Forschungsgemeinschaft (DFG) in the framework of the project 528378584 on “Under Voltage Control: Nb₂O₅ Based Locally Active Threshold Switches,” which is part of the Collaborative Research Centres (CRC)/Transregios (TRR) programme 528378584 “TRR 404: Next Generation Electronics with Active Devices in Three Dimensions (Active-3D)”.

REFERENCES

- [1] M.D. Pickett, and R.S. Williams, “Sub-100 fJ and sub-nanosecond thermally driven threshold switching in niobium oxide crosspoint nanodevices,” *Nanotechnology*, vol. 23, no. 21, 215202(9pp.), 2012
- [2] A. Ascoli, S. Slesazek, H. Mähne, R. Tetzlaff, and T. Mikolajick, “Nonlinear dynamics of a locally-active memristor,” *IEEE Trans. Circuits and Systems-I: Regular Papers*, vol. 62, no. 4, pp. 1165-1174, 2015
- [3] M.-K. Song, J.-H. Kang, X. Zhang, W. Ji, A. Ascoli, I. Messaris, A.S. Demirkol, B. Dong, S. Aggarwal, W. Wan, S.-M. Hong, S.G. Cardwell, I. Boybat, J.-s. Seo, J.-S. Lee, M. Lanza, H. Yeon, M. Onen, J. Li, B. Yildiz, J.A. del Alamo, S. Kim, S. Choi, G. Milano, C. Ricciardi, L. Alff, Y. Chai, Z. Wang, H. Bhaskaran, M.C. Hersam, D. Strukov, H.-S. P. Wong, I. Valov, B. Gao, H. Wu, R. Tetzlaff, A. Sebastian, W. Lu, L. Chua, J.J. Yang, and J. Kim, “Recent Advances and Future Prospects for Memristive Materials, Devices, and Systems,” *American Chemical Society (ACS) Nano*, vol. 17, no. 13, pp. 11994-12039, 2023, DOI: 10.1021/acsnano.3c03505
- [4] G.A. Gibson, S. Musunuru, J. Zhang, K. Vandenberghe, J. Lee, C.-C. Hsieh, W. Jackson, Y. Jeon, D. Henze, Z. Li, and R.S. Williams, “An accurate locally active memristor model for S-type negative differential resistance in NbOx,” *Applied Physics Letters*, vol. 108, no. 2, 023505 (5pp.), 2016
- [5] L.O. Chua, “Local Activity is the Origin of Complexity,” *Int. J. on Bifurcation and Chaos*, vol. 15, no. 11, pp. 3435-3456, 2005
- [6] A. Ascoli, S.A. Demirkol, R. Tetzlaff, S. Slesazek, T. Mikolajick, and L.O. Chua, “On Local Activity and Edge of Chaos in a NaMLab Memristor,” *Frontiers in Neuroscience*, vol. 15, no. 651452, (30pp.), 2021
- [7] A. Ascoli, A.S. Demirkol, R. Tetzlaff, and L.O. Chua, “Edge of Chaos is Sine Qua Non for Turing Instability,” *IEEE Trans. Circuits and Systems-I (TCAS-I): Regular Papers*, vol. 69, no. 11, pp. 4596-4609, Nov. 2022

- [8] A.S. Demirkol, A. Ascoli, I. Messaris, V. Ntinis, D. Prousalis, and R. Tetzlaff, "A Fast and Compact Threshold Switch Based Cellular Nonlinear Network Cell," *IEEE Trans. on Circuits and Systems-I (TCAS-I)*, 2025, submitted
- [9] A. Ascoli, A.S. Demirkol, I. Messaris, V. Ntinis, D. Prousalis, S. Slesazek, T. Mikolajick, F. Corinto, M. Bonnin, M. Gilli, P.P. Civalleri, R. Tetzlaff, and L. Chua, "Edge of Chaos Theory Unveils the First and Simplest Ever Reported Hodgkin-Huxley Neuristor," *Adv. Ele. Mat.*, 2025, DOI:10.1002/aelm.202400789
- [10] M. Weiher, M. Herzig, R. Tetzlaff, A. Ascoli, T. Mikolajick, and S. Slesazek, "Improved Vertex Coloring With NbOx Memristor-Based Oscillatory Networks," *IEEE Trans. on Circuits and Systems-I: Regular Papers*, vol. 68, no. 5, pp. 2082-2095, 2021
- [11] H. Mähne, H. Wylezich, S. Slesazek, T. Mikolajick, J. Vesely, V. Klemm, D. Rafaja, "Room temperature fabricated NbOx/Nb2O5 memory switching device with threshold switching effect," 5th IEEE International Memory Workshop, 2013
- [12] S. Slesazek, H. Mähne, H. Wylezich, A. Wachowiak, J. Radhakrishnan, A. Ascoli, R. Tetzlaff, and T. Mikolajick, "Physical model of threshold switching in NbO2 based memristors," *Journal of the Royal Society of Chemistry*, vol. 5, no. 124, pp. 102318-102322, 2015
- [13] <https://www.namslab.com>
- [14] L.O. Chua, C.A. Desoer, and E.A. Kuh, "Linear and nonlinear circuits," McGraw Hill, New York, 1987, ISBN: 0-07-010898-6
- [15] A.S. Demirkol, A. Ascoli, I. Messaris, and R. Tetzlaff, "Pattern Formation in an RD-MCNN with Locally Active Memristors," in *Memristor - An Emerging Device for Post-Moore's Computing and Applications*, Yao- Feng Chang ed., IntechOpen Limited, London, 2021, DOI: 10.5772/intechopen.100463
- [16] H.K. Khalil, "Nonlinear Systems," third edition, Pearson, 768pp., ISBN-13: 978-0130673893
- [17] M. Rao, H. Tang, J. Wu, W. Song, M. Zhang, W. Yin, Y. Zhuo, F. Kiani, B. Chen, X. Jiang, H. Liu, H.-Y. Chen, R. Midya, F. Ye, H. Jiang, Z. Wang, M. Wu, M. Hu, H. Wang, Q. Xia, N. Ge, J. Li, and J.J. Yang, "Thousands of conductance levels in memristors integrated on CMOS," *Nature*, vol. 615, no. 7954, pp. 823-829, 2023
- [18] D. Sharma, S.P. Rath, B. Kundu, A. Korkmaz, H. S, D. Thompson, N. Bhat, S. Goswami, R.S. Williams, and S. Goswami, "Linear symmetric self-selecting 14-bit kinetic molecular memristors," *Nature*, vol. 633, pp. 560-566, 2024
- [19] A. Ascoli, A.S. Demirkol, R. Tetzlaff, and L.O. Chua, "Edge of Chaos Theory Sheds Light into the All-or-None Phenomenon in Neurons - Part I: On the Fundamental Role of the Sodium Ion Channel," *IEEE Trans. Circuits and Systems-I (TCAS-I): Regular Papers*, vol. 71, no. 1, pp. 5-19, 2024, DOI: 10.1109/TCSI.2023.3339240
- [20] M.D. Pickett, and R.S. Williams, "Phase transitions enable computational universality in neuristor-based cellular automata," *Nanotechnology*, vol. 24, 384002(7pp.), 2013, DOI: 10.1088/0957-4484/24/38/384002
- [21] A. Ascoli, A.S. Demirkol, R. Tetzlaff, and L.O. Chua, "Analysis and Design of Bio-Inspired Circuits with Locally-Active Memristors," *IEEE Trans. Circuits and Systems-II (TCAS-II): Express Briefs*, vol. 71, no. 3, pp. 1721-1726, March 2024, DOI: 10.1109/TCSII.2023.3339535
- [22] A. Ascoli, A.S. Demirkol, R. Tetzlaff, and L.O. Chua, "Edge of Chaos Theory Resolves Smale Paradox," *IEEE Trans. Circuits and Systems-I (TCAS-I): Regular Papers*, vol. 69, no. 3, pp. 1252-1265, 2022
- [23] A. Ascoli, A.S. Demirkol, I. Messaris, V. Ntinis, D. Prousalis, S. Slesazek, T. Mikolajick, F. Corinto, E. Gemo, M. Bonnin, M. Gilli, P.P. Civalleri, R. Tetzlaff, and L. Chua, "A Memristor on Edge of Chaos Enables to Reproduce the Entire Life Cycle of an Action Potential across the Hodgkin- Huxley Neuron in a Three-Element Cell featuring Half the Number of Degrees of Freedom," *ACS Nano*, 2025
- [24] A. Ascoli, A.S. Demirkol, I. Messaris, V. Ntinis, D. Prousalis, S. Slesazek, T. Mikolajick, E. Gemo, F. Corinto, M. Bonnin, M. Gilli, P.P. Civalleri, R. Tetzlaff, and L. Chua, "The Hodgkin-Huxley Neuristor," *Proceedings of the International Joint Conference on Neural Networks (IJCNN)*, Rome, July 2025